The Canadian Mineralogist
Vol. 46, pp. 1443-1454 (2008)
DOI : 10.3749/canmin.46.6.1443

COMPRESSIBILITY AND HIGH-PRESSURE BEHAVIOR OF $Ab_{63}Or_{27}An_{10}$ ANORTHOCLASE

Fabrizio NESTOLA[§]

Dipartimento di Geoscienze, Università di Padova, Via Giotto 1, I–35137 Padova, Italy

Nadia CURETTI, Piera BENNA and Gabriella IVALDI

Dipartimento di Scienze Mineralogiche e Petrologiche, Università di Torino, Via Valperga Caluso 35, I–10125 Torino, Italy

Ross J. ANGEL

Department of Geosciences, Virginia Polytechnic Institute and State University, Blacksburg, Virginia 24061, U.S.A.

Emiliano BRUNO

Dipartimento di Scienze Mineralogiche e Petrologiche, Università di Torino, Via Valperga Caluso 35, I–10125 Torino, Italy

Abstract

A natural sample of anorthoclase of composition $Na_{0.63}K_{0.27}Ca_{0.10}Al_{1.10}Si_{2.90}O_8$ ($Ab_{63}Or_{27}An_{10}$) was treated at T = 950°C for one week, and then investigated by single-crystal X-ray diffraction *in situ* at high pressure using a diamond-anvil cell. After the thermal treatment, the unit-cell parameters at room pressure and temperature are a 8.2523(3), b 12.9363(5), c 7.1416(3) Å, α 92.046(5), β 116.294(3), γ 90.206(4)°, V 682.91(5) Å^3, and indicate nearly complete Al–Si disorder. Unit-cell parameters were measured at room temperature as a function of pressure to 8.48 GPa. The P–V data are described by a fourth-order Birch–Murnaghan equation of state with the following coefficients: V_0 = 682.92(5) Å^3, K_{T0} = 54.4(4) GPa, K' = 6.4(3), K'' = –1.16(12) GPa^{-1}. The unit-cell compression is anisotropic, as indicated by the unit strain tensors, with 53% of the total compression over the entire range in pressure accommodated along a direction close to **a***. The axial linear compressibilities (β_a = 6.92, β_b = 2.83 and β_c = 3.91 × 10^{-3} GPa^{-1}) reflect a compressibility pattern similar to that of other alkali feldspars. The X-ray intensity data were collected at a pressure of 0.0001, 4.7 and 6 GPa. The results of the refinements indicate that the symmetry of this anorthoclase remains triclinic, $C\overline{1}$, over the entire range in pressure; no phase transitions were observed. The pressure causes a strong deformation of the extra-framework M site, with a contraction of the volume by 16% at P = 6 GPa. The compression is accompanied by a decrease of the M–O distances and a possible increase in the coordination number of the non-tetrahedrally coordinated cations from "5+1" to "5+2", related to the significant decrease of the M–OC(m) distance. The increase of the coordination number is not associated with any phase transition. Together with the deformation of the M site, the inter-tetrahedron tilting of essentially rigid tetrahedra (detectable by the changes in the T–O–T angles) is the main mechanism of compression of the structure of anorthoclase.

Keywords: anorthoclase, X-ray diffraction, single crystal, high pressure.

Sommaire

Nous avons chauffé un échantillon naturel d'anorthoclase de composition $Na_{0.63}K_{0.27}Ca_{0.10}Al_{1.10}Si_{2.90}O_8$ ($Ab_{63}Or_{27}An_{10}$) à 950°C pour une semaine, et nous l'avons ensuite étudié par diffraction X *in situ* à pression élevée au moyen d'une cellule à enclumes de diamant. Après le traitement thermique, les paramètres réticulaires à pression et température ambiantes sont a 8.2523(3), b 12.9363(5), c 7.1416(3) Å, α 92.046(5), β 116.294(3), γ 90.206(4)°, V 682.91(5) Å^3, et témoignent d'un désordre Al–Si presque complet. Nous avons mesuré les paramètres à température de la pièce en fonction de la pression jusqu'à 8.48 GPa. On peut décrire les données P–V par une équation d'état Birch–Murnaghan du quatrième ordre, avec les coefficients suivants: V_0 = 682.92(5) Å^3, K_{T0} = 54.4(4) GPa, K' = 6.4(3), K'' = –1.16(12) GPa^{-1}. La compression de la maille élémentaire est anisotrope, telle qu'indiquée par les tenseurs unitaires de déformation, avec 53% de la compression totale sur l'intervalle de pression étudié accommodé le long d'une direction voisine de **a***. Les compressibilités axiales linéaires (β_a = 6.92, β_b = 2.83 et β_c = 3.91, toutes

---

[§] *E-mail address*: fabrizio.nestola@unipd.it

$\times$ 10^{-3} GPa^{-1}) ressemblent au schéma de compressibilité des autres feldspaths alcalins. Les données sur l'intensité en diffraction X ont été prélevées à 0.0001, 4.7 et 6 GPa. Les résultats des affinements montrent que la symétrie de ce cristal d'anorthoclase demeure triclinique, $C\bar{1}$, sur tout l'intervalle de pression étudié; il n'y aucune inversion. La pression cause une forte déformation du site *M* externe à la trame, avec contraction de son volume de 16% à 6 GPa. La compression mène à une diminution des distances *M*–O et une augmentation possible de la coordinence des cations non tétracoordonnés, de "5+1" à "5+2", liée à la diminution importante de la distance *M*–OC(m). L'augmentation de la coordinence n'est pas associée à une inversion. De concert avec la déformation du site *M*, l'inclinaison des tétraèdres essentiellement rigides, décelée par les changements des angles *T*–O–*T*, serait le mécanisme principal pour expliquer la compression de la structure de l'anorthoclase.

(Traduit par la Rédaction)

Mots-clés: anorthoclase, diffraction X, monocristal, pression élevée.

INTRODUCTION

The definitive texts on the crystal chemistry of feldspars are the two editions of "Feldspar Minerals" (Smith 1974a, b, Smith & Brown 1988). One of the topics absent from the first edition, and only briefly touched upon in the second edition, is the behavior of feldspars under high pressures. This reflects the fact that the techniques for high-pressure diffraction studies were only developed in the period between the publication of the two volumes. The initial experiments on feldspars by Hazen (1976) immediately revealed complexities in their behavior at high pressure. Continuing improvements in accessible range of pressure and experimental precision have only served to identify further complexities. Very recent experiments, for example, have documented elastic softening in albite (Benusa *et al.* 2005) and completely new symmetries and sequences of phase transformations for feldspars (Nestola *et al.* 2004, Benna *et al.* 2007). These results remind one of the warning implicit in the title of an early paper by J.V. Smith: "*Further complexities* in the lamellar structure of alkali feldspars" (Smith & MacKenzie 1954).

For the alkali feldspars, several questions remain open with respect to their high-pressure behavior. First, what are the effects of changes in composition and state of Al,Si order on the elastic properties and equations of state? There does seem to be a general trend of increasing bulk modulus with K content (Allan & Angel 1997, Angel *et al.* 1988, Benusa *et al.* 2005, Tenner *et al.* 2007). Data for sanidine and microcline suggest that disorder softens the structure (Allan & Angel 1997, Angel *et al.* 1988), whereas in albite, the bulk modulus increases with disorder (Tenner *et al.* 2007). Second, there still remains the question of whether alkali feldspars undergo phase transitions at high pressures related to reconfigurations of the framework, without changes in Al,Si order. Hazen (1976) found a monoclinic–triclinic phase transformation below 2 GPa in sanidine samples of intermediate compositions ($Or_{67}Ab_{31}An_2$ and $Or_{82}Ab_{17}An_1$), whereas Angel *et al.* (1988) did not find any phase transitions in $Or_{98}Ab_2$ sanidine up to 5 GPa. On the other hand, the structural changes in albite above 9 GPa (Benusa *et al.* 2005) could be described as a form of elastic phase transition. Third, what are the atomic-scale changes in structure that form the basis of the observed changes in macroscopic and thermodynamic properties? For the alkali feldspars, only the structures of the ordered end-members albite (Downs *et al.* 1994, Benusa *et al.* 2005) and microcline (Allan & Angel 1997) have been determined at high pressures. In order to provide some further data in an attempt to resolve these questions, we have investigated at high pressure a sample of anorthoclase of composition $Na_{0.63}K_{0.27}Ca_{0.10}Al_{1.10}Si_{2.90}O_8$, thermally treated at 950°C to induce Al,Si disorder.

EXPERIMENTAL

The anorthoclase investigated in this work, of the composition $Ab_{63}Or_{27}An_{10}$, is from a trachyte from Zovon di Vò, Colli Euganei, Padova, Italy, and was taken from the collection of the Museo Regionale di Scienze Naturali, Torino, Italy. The samples were annealed at T = 950°C for one week in an electric furnace, and then quenched in air. After the thermal treatment, the unit-cell parameters at room pressure and temperature are *a* 8.2523(3), *b* 12.9363(5), *c* 7.1416(3) Å, α 92.046(5)°, β 116.294(3)°, γ 90.206(4)°, *V* 682.91(5) Å^3, indicating nearly complete Al,Si disorder. The crystals were selected on the basis of their sharp optical extinction, absence of twinning, transparency, absence of defects visible with an optical microscope and sharpness of diffraction peaks. The chemical composition of the crystal was obtained using an EDAX Genesis 4000 XMS microprobe (ΔV = 20 kV, WD = 24 mm, adsorbed current 190 pA, spot size = 248.6 nm) and the following standards: albite for Na, K-rich celsian for Si, Al, K, uvarovite for Ca.

One crystal was loaded in a ETH design of diamond-anvil cell (DAC) (Miletich *et al.* 2000) with a T301 steel gasket pre-indented to 85 μm with a 300 μm hole. A 4:1 methanol:ethanol mixture was used as the pressure-transmitting medium. Quartz was used as an internal pressure standard (Angel *et al.* 1997). The unit-cell parameters (Table 1) were determined at room temperature in the pressure range 0.0001–8.48 GPa from the setting angles of 19–21 reflections centered in eight positions (King & Finger 1979) using a Huber four-circle diffractometer with a point detector (Angel *et al.* 1997, 2000).

Another crystal (140 × 120 × 40 μm) of the same sample was loaded in the DAC using the same experimental conditions (gasket pre-indented to 110 μm with a 250 μm hole), but without a pressure standard, and complete intensity data were measured at room pressure (crystal in the DAC), at $P = 4.7$ and 6.0 GPa (these pressures were calculated using the equation of state determined in the experiment performed using the point detector). Intensity data were collected using a STOE single-crystal diffractometer with graphite-monochromated Mo$K\alpha$ radiation and an Oxford Diffraction CCD detector over the range $5 \leq 2\theta \leq 60°$ using a 0.2° ω-scan with an exposure time of 60 s per frame. The sample–detector distance was 60 mm. The CRYSALISRED^{TM} program (Oxford Diffraction) was used to integrate the intensity data and to apply the Lorentz-polarization correction, whereas X-RED (Stoe & Cie 2001) and X-SHAPE (Stoe & Cie 1999) programs were used to correct for absorption. The size of gasket and crystal were such that diffraction peaks were not affected by gasket shadowing (Angel *et al.* 2000); the absorption correction applied in this work gave reliable results. Weighted structural refinements were done in $C\overline{1}$ space group at all pressures (since no violations of this symmetry were detected) using the SHELX–97 package (Sheldrick 2008) starting from the atomic coordinates of $Or_{33}Ab_{67}An_1$ anorthoclase of Harlow (1982). The *M*-site occupancies were fixed to those determined from the chemical analyses. Only the *M* site was refined with anisotropic displacement parameters under pressure. Refinement details and crystal-structure data are reported in Table 2, whereas atomic coordinates and thermal parameters are shown in Table 3. Selected bond-lengths, polyhedron volumes, O–*T*–O and *T*–O–*T* angles are listed in Tables 4, 5 and 6, respectively. Tables of structure factors are available from the Depository of Unpublished Data on the MAC website [document Anorthoclase CM46_1443].

RESULTS AND DISCUSSION

Equation of state and elasticity

The evolution of the unit-cell parameters and volume as a function of pressure was measured at 15 different pressures up to 8.48 GPa. They are reported in Table 1 and Figures 1 and 2. The *a*, *b*, and *c* unit-cell parameters decrease non-linearly with increasing pressure without discontinuities, indicating that no phase transition occurs in the pressure range investigated. They show a linear negative variation by 6.2, 2.4 and 3.4%, respectively, to the maximum pressure reached. The axial linear compressibilities for anorthoclase are $\beta_a = 6.92$, $\beta_b = 2.83$ and $\beta_c = 3.91 \times 10^{-3}$ GPa^{-1} (Table 7), indicating strong axial anisotropy ($\Delta a/a_0 : \Delta b/b_0 : \Delta c/c_0 = 2.44{:}1{:}1.38$). This pattern of anisotropy is similar to that observed for the other alkali feldspars studied at high pressure (Table 7). However, slight differences are present in the degree of the anisotropy among alkali feldspars: the linear axial compressibility ratio for our sample is very similar to that of low albite (~2.8:1:1.1, Downs *et al.* 1994, Benusa *et al.* 2005), whereas it is much less anisotropic than sanidine (5.2:1:2.4, Angel *et al.* 1988) or microcline (7.7:1:3.7, Allan & Angel 1997).

The pattern of change in the unit-cell angles α, β, and γ is distinct from both albite and microcline in that the α angle increases with pressure, whereas it decreases with pressure in both end-members. However, the plateau in the β angle variation found in both end-members is also present in anorthoclase; this plateau was associated with bonding changes in microcline (Allan & Angel 1997), but that is clearly not the cause

TABLE 1. UNIT-CELL PARAMETERS AND VOLUME *VERSUS* PRESSURE FOR ANORTHOCLASE $Ab_{63}Or_{27}An_{10}$

P(GPa)	a (Å)	*b* (Å)	*c* (Å)	α (°)	β (°)	γ (°)	*V*(Å^3)
0.00010(1)	8.2523(3)	12.9363(5)	7.1416(3)	92.046(5)	116.294(3)	90.206(4)	682.91(5)
1.078(5)	8.1782(4)	12.8871(7)	7.1074(2)	92.317(4)	116.384(3)	90.311(5)	670.27(5)
1.796(5)	8.1324(4)	12.8572(7)	7.0861(4)	92.445(6)	116.423(3)	90.376(5)	662.65(6)
2.699(7)	8.0780(5)	12.8217(9)	7.0590(4)	92.552(7)	116.450(4)	90.457(7)	653.63(6)
3.075(8)	8.0558(5)	12.8070(9)	7.0486(3)	92.580(7)	116.457(4)	90.495(6)	650.05(6)
3.895(6)	8.0095(4)	12.7768(7)	7.0255(3)	92.634(5)	116.468(3)	90.571(6)	642.55(5)
4.387(6)	7.9815(4)	12.7586(6)	7.0121(3)	92.644(5)	116.470(3)	90.626(6)	638.13(5)
4.891(7)	7.9548(4)	12.7424(6)	6.9994(4)	92.649(6)	116.468(3)	90.671(5)	634.03(5)
5.370(7)	7.9292(5)	12.7256(6)	6.9864(4)	92.654(7)	116.463(4)	90.714(7)	629.98(6)
5.787(7)	7.9077(4)	12.7117(6)	6.9754(4)	92.652(7)	116.461(4)	90.764(6)	626.59(5)
6.385(5)	7.8754(4)	12.6926(6)	6.9600(3)	92.639(5)	116.449(3)	90.813(5)	621.77(5)
6.910(8)	7.8482(4)	12.6750(6)	6.9466(4)	92.618(6)	116.450(3)	90.854(5)	617.56(5)
7.464(8)	7.8204(4)	12.6569(7)	6.9314(4)	92.590(7)	116.437(4)	90.918(6)	613.20(6)
7.980(9)	7.7942(4)	12.6425(9)	6.9184(4)	92.568(7)	116.433(4)	90.944(6)	609.34(5)
8.482(10)	7.7679(3)	12.6262(8)	6.9046(3)	92.527(6)	116.431(3)	90.987(5)	605.31(5)

of the plateau in albite. Note that the increase in both α and γ angles, away from 90°, indicates that pressure increases the deviation from the archetypal monoclinic symmetry of feldspars.

The strain induced by increasing pressure has been evaluated by the use of the STRAIN program written by Ohashi (1982). The magnitudes and orientations of the principal axes of the strain ellipsoid, calculated from the cell parameters, are reported in Table 7. The compression in anorthoclase is anisotropic, with 53% of the total compression over the entire range of pressure accommodated along a direction very close to **a***. This orientation of the strain ellipsoid, with the most compressible direction about 15–20° from the (100) plane normal, corresponds approximately to that observed in all other feldspars studied at high pressure (Angel 1994). An examination of the magnitudes of the principal axes of the strain ellipsoid shows that in the pressure range 0–8.48 GPa, among these feldspars, our anorthoclase is the least anisotropic (53% of the total compression along the ε_1 axis), whereas microcline is the most anisotropic (65%).

When the *P–V* data are transformed to an $F_E - f_E$ plot (Fig. 3), where F_E is the "normalized pressure" and is $\sim P / 3 \times f_E \times (1 + 2 f_E)^{5/2}$, with f_E defined as the "normalized strain", $f_E = [(V_0 / V)^{2/3} - 1] / 2$, they clearly fall on a curve. This indicates (*e.g.*, Angel 2000) that the data can only be represented by a fourth-order Birch–Murnaghan EoS, as was found for albite (Benusa *et al.*

TABLE 2. REFINEMENT DETAILS AND CRYSTAL-STRUCTURE DATA FOR ANORTHOCLASE $Ab_{63}Or_{27}An_{10}$

P (GPa)	0.0001	4.7	6.0
a (Å)	8.278(13)	7.959(5)	7.890(7)
b (Å)	12.949(14)	12.767(4)	12.720(6)
c (Å)	7.145(12)	6.999(8)	6.960(8)
α (°)	91.79(15)	92.51(6)	92.46(7)
β (°)	116.16(16)	116.50(8)	116.53(10)
γ (°)	90.19(12)	90.69(4)	90.83(6)
V (Å³)	686.97	635.46	623.94
Space group	$C\bar{1}$	$C\bar{1}$	$C\bar{1}$
R_1	8.44	8.83	8.57
Unique reflections	430	419	415
S	1.2	1.1	1.1

TABLE 3. ATOM COORDINATES AND ISOTROPIC THERMAL PARAMETERS (Å²) FOR ANORTHOCLASE $Ab_{63}Or_{27}An_{10}$ AT VARIOUS PRESSURES

P (GPa)		0.0001	4.7	6.0			0.0001	4.7	6.0
M	*x*	0.2751(12)	0.2616(10)	0.2593(10)	OB(0)	*x*	0.8262(21)	0.8087(21)	0.8045(23)
	y	0.0027(5)	0.0050(5)	0.0050(5)		*y*	0.1246(8)	0.1058(8)	0.1038(9)
	z	0.1369(30)	0.1356(27)	0.1378(26)		*z*	0.2218(42)	0.1960(41)	0.1936(43)
	U_{eq}	0.079(15)	0.053(7)	0.050(12)		U_{iso}	0.032(3)	0.037(3)	0.048(4)
*T*1(0)	*x*	0.0061(9)	0.0018(8)	0.0018(9)	OB(m)	*x*	0.8250(22)	0.8072(21)	0.7976(24)
	y	0.1737(3)	0.1674(3)	0.1666(3)		*y*	0.8590(9)	0.8503(9)	0.8494(9)
	z	0.2165(18)	0.2165(19)	0.2208(20)		*z*	0.2378(43)	0.2329(42)	0.2201(46)
	U_{iso}	0.023(1)	0.021(1)	0.024(1)		U_{iso}	0.037(3)	0.035(3)	0.040(3)
*T*1(m)	*x*	0.0043(9)	-0.0033(8)	-0.0071(8)	OC(0)	*x*	0.0212(21)	-0.0012(18)	-0.0095(19)
	y	0.8178(3)	0.8147(3)	0.8144(3)		*y*	0.2998(8)	0.2925(7)	0.2925(7)
	z	0.2213(19)	0.2248(19)	0.2222(18)		*z*	0.2625(46)	0.2719(43)	0.2700(43)
	U_{iso}	0.028(1)	0.021(1)	0.020(1)		U_{iso}	0.036(3)	0.026(3)	0.026(3)
*T*2(0)	*x*	0.6969(11)	0.6850(9)	0.6838(9)	OC(m)	*x*	0.0262(22)	0.0093(18)	0.0052(19)
	y	0.1139(3)	0.1085(3)	0.1074(3)		*y*	0.6915(8)	0.6873(7)	0.6872(7)
	z	0.3392(23)	0.3246(20)	0.3259(19)		*z*	0.2441(50)	0.2235(43)	0.2226(43)
	U_{iso}	0.024(1)	0.022(1)	0.022(1)		U_{iso}	0.044(4)	0.024(3)	0.030(3)
*T*2(m)	*x*	0.6938(11)	0.6767(10)	0.6716(10)	OD(0)	*x*	0.1889(17)	0.1901(18)	0.1928(20)
	y	0.8814(3)	0.8771(3)	0.8764(3)		*y*	0.1184(8)	0.1181(9)	0.1179(9)
	z	0.3492(23)	0.3568(21)	0.3518(23)		*z*	0.3917(32)	0.3925(30)	0.3950(31)
	U_{iso}	0.022(1)	0.021(1)	0.022(1)		U_{iso}	0.034(4)	0.043(4)	0.049(4)
OA(1)	*x*	0.0002(21)	0.0025(19)	0.0047(19)	OD(m)	*x*	0.1861(19)	0.1798(17)	0.1752(17)
	y	0.1362(9)	0.1351(9)	0.1351(9)		*y*	0.8727(10)	0.8706(8)	0.8713(9)
	z	0.9934(28)	0.9830(28)	0.9871(29)		*z*	0.4065(32)	0.4104(29)	0.4119(29)
	U_{iso}	0.046(4)	0.036(3)	0.036(3)		U_{iso}	0.049(5)	0.030(3)	0.038(3)
OA(2)	*x*	0.6040(20)	0.5795(17)	0.5737(18)					
	y	0.9967(7)	0.9917(7)	0.9908(6)					
	z	0.2817(44)	0.2826(40)	0.2765(38)					
	U_{iso}	0.034(3)	0.026(3)	0.026(3)					

For the *M* site, the value of U_{eq} is reported, as this site was refined with anisotropic displacement parameters.

TABLE 4. *M*-O AND *T*-O BOND DISTANCES (Å) AND POLYHEDRON VOLUMES (Å^3) FOR ANORTHOCLASE $Ab_{63}Or_{27}An_{10}$ AS A FUNCTION OF PRESSURE

P (GPa)	0.0001	4.7	6.0		0.0001	4.7	6.0
M-OA(1)	2.700(18)	2.534(15)	2.497(15)	*T*1(0)-OA(1)	1.631(16)	1.671(16)	1.669(16)
M-OA(1)	2.701(17)	2.555(14)	2.532(13)	*T*1(0)-OB(0)	1.633(10)	1.663(10)	1.668(11)
M-OA(2)	2.452(18)	2.279(14)	2.238(15)	*T*1(0)-OC(0)	1.648(11)	1.630(10)	1.635(10)
M-OB(0)	2.797(28)	2.497(27)	2.482(26)	*T*1(0)-OD(0)	1.662(16)	1.613(15)	1.607(15)
M-OB(m)	3.069(27)	3.090(26)	3.043(28)	<*T*1(0)-O>	1.644	1.644	1.645
M-OC(0)	3.229(16)	3.252(14)	3.216(15)				
M-OC(m)	3.054(17)	2.892(11)	2.866(12)	*T*1(m)-OA(1)	1.649(16)	1.617(15)	1.625(16)
M-OD(0)	2.656(20)	2.520(19)	2.487(18)	*T*1(m)-OB(m)	1.630(10)	1.604(10)	1.604(10)
M-OD(m)	2.922(21)	2.907(20)	2.890(20)	*T*1(m)-OC(m)	1.652(11)	1.631(10)	1.623(10)
				*T*1(m)-OD(m)	1.643(17)	1.589(15)	1.590(15)
<$^{[6]}$*M*-O>	2.705	2.549	2.521	<*T*1(m)-O>	1.644	1.610	1.610
<$^{[7]}$*M*-O>	2.755	2.598	2.570				
<$^{[8]}$*M*-O>	2.794	2.659	2.629	*T*2(0)-OA(2)	1.655(12)	1.650(10)	1.651(10)
				*T*2(0)-OB(0)	1.634(14)	1.603(15)	1.593(15)
V(*M*O6)	18.2(3)	17.0(3)	16.4(4)	*T*2(0)-OC(m)	1.635(15)	1.638(13)	1.653(14)
V(*M*O7)	25.7(5)	22.5(4)	21.9(4)	*T*2(0)-OD(m)	1.642(18)	1.684(17)	1.666(17)
V(*M*O8)	31.6(6)	27.4(5)	26.5(5)	<*T*2(0)-O>	1.642	1.644	1.641
				*T*2(m) -OA(2)	1.658(12)	1.657(12)	1.650(12)
				*T*2(m)-OB(m)	1.627(14)	1.654(15)	1.656(14)
				*T*2(m) -OC(0)	1.646(14)	1.637(11)	1.638(11)
				*T*2(m) -OD(0)	1.669(17)	1.592(17)	1.599(17)
				<*T*2(m)-O>	1.650	1.635	1.636

TABLE 5. O-*T*-O ANGLES (°) IN ANORTHOCLASE $Ab_{63}Or_{27}An_{10}$ AT VARIOUS PRESSURES

*T*1(0)	OA(1)-OB(0)	OA(1)-OC(0)	OA(1)-OD(0)	OB(0)-OC(0)	OB(0)-OD(0)	OC(0)-OD(0)
0.0001 GPa	107.10	114.60	103.84	111.41	108.13	111.28
4.7	103.24	115.92	104.42	110.70	111.96	110.33
6.0	102.54	114.98	103.37	109.60	113.54	112.41
*T*1(m)	OA(1)-OB(m)	OA(1)-OC(m)	OA(1)-OD(m)	OB(m)-OC(m)	OB(m)-OD(m)	OC(m)-OD(m)
0.0001 GPa	106.44	116.63	103.50	113.27	109.14	107.26
4.7	106.60	113.87	100.84	110.71	112.75	111.69
6.0	105.20	114.21	101.43	110.30	113.43	111.89
*T*2(0)	OA(2)-OB(0)	OA(2)-OC(m)	OA(2)-OD(m)	OB(0)-OC(m)	OB(0)-OD(m)	OC(m)-OD(m)
0.0001 GPa	106.92	106.41	107.26	110.16	112.58	113.08
4.7	106.70	103.16	108.19	112.34	111.52	114.26
6.0	105.27	102.22	110.61	111.79	110.78	115.37
*T*2(m)	OA(2)-OB(m)	OA(2)-OC(0)	OA(2)-OD(0)	OB(m)-OC(0)	OB(m)-OD(0)	OC(0)-OD(0)
0.0001 GPa	108.18	106.18	109.18	110.69	111.45	110.97
4.7	108.86	104.55	110.41	109.44	107.94	115.49
6.0	108.06	103.96	110.36	109.48	109.57	115.09

The errors are between 0.5 and 1°.

2005). A weighted fit of the data yields the following coefficients: V_0= 682.92(5) Å^3, K_{T0} = 54.4(4) GPa, K' = 6.4(3), K'' = –1.16(12) GPa^{-1}. These values suggest that the softening found in albite above 5 GPa (Benusa *et al.* 2005) occurs above 8 GPa in this anorthoclase.

The disordered anorthoclase is therefore significantly softer than either disordered high albite [K_{T0} = 56.4(7) GPa; Tenner *et al.* 2007] or sanidine [57(1) GPa; Angel 1994]. However the present anorthoclase is approximately as stiff as would be expected by linear interpolation of K_{T0} between the ordered end-members albite [K_{T0} = 52.3(9) GPa; Benusa *et al.* 2005] and microcline [K_{T0} = 58(2) GPa; Allan & Angel 1997]. These data clearly indicate that the interplay between the elastic effects of compositional change and degree of order in alkali feldspars has still not been resolved, and that the current results cannot be rationalized by simple linear interpolations between the current data available for the end-member compositions. One alternative explanation is that the earlier EoS data on alkali feldspars may be either of insufficient precision, or in error.

TABLE 6. *T*–O–*T* BOND ANGLES (°) IN ANORTHOCLASE $Ab_{63}Or_{27}An_{10}$ AT VARIOUS PRESSURES

P (GPa)	0.0001	4.7	6.0
*T*1(0)-OA(1)-*T*1(m)	141.21	142.38	142.84
*T*2(m)-OA(2)-*T*2(0)	132.32	128.17	126.98
*T*1(0)-OB(0)-*T*2(0)	149.23	136.50	134.20
*T*1(m)-OB(m)-*T*2(m)	155.90	153.51	149.67
*T*1(0)-OC(0)-*T*2(m)	132.24	126.71	123.95
*T*1(m)-OC(m)-*T*2(0)	136.16	133.07	133.09
*T*1(0)-OD(0)-*T*2(m)	137.79	141.44	140.74
*T*1(m)-OD(m)-*T*2(0)	142.94	147.29	149.72

The errors are between 0.5 and 1°.

Crystal-structure evolution

The M site: The *M* cation at room pressure in our sample is coordinated with bonds of 2.70 Å or less to four atoms of oxygen, two OA(1), OD(0) and OA(2). The fifth shortest distance is to OB(0) at 2.80(3) Å. These provide the same bonded environment as that found in albite and microcline at room pressure, although all of the distances are significantly longer than found in albite and shorter than those found in microcline, as expected for the intermediate occupancy of the *M* site by Na and K in anorthoclase. The next shortest distance is *M*–OD(m) at 2.92 Å, which would make the coordination better described as "5+1" (Table 4), again intermediate between albite [in which OD(m) is not bonded to Na] and microcline [in which OD(m) is

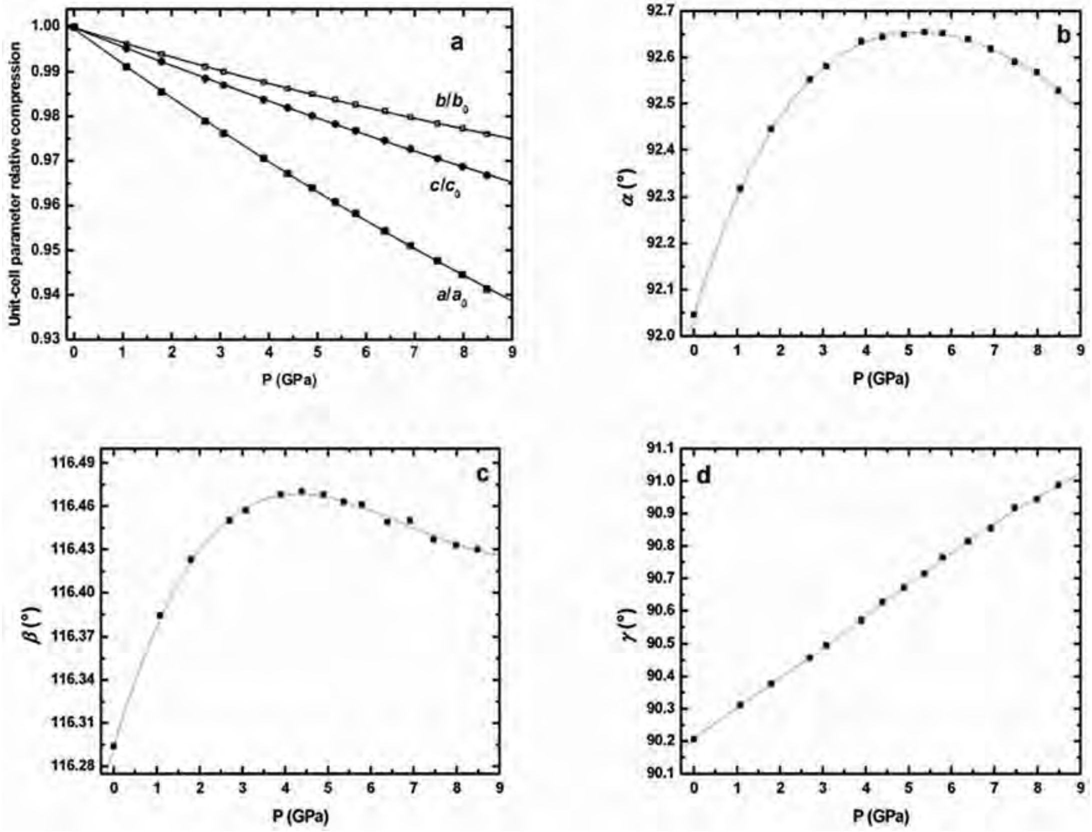

FIG. 1. (a) Relative compression of the *a*, *b* and *c* unit-cell parameters. Lines are the equation of state fit to the linear data. (b, c, d) Evolution of the unit-cell angles with pressure for anorthoclase. Lines are smoothed interpolations through the data. Symbol sizes exceed the estimated uncertainties of the data in all figures.

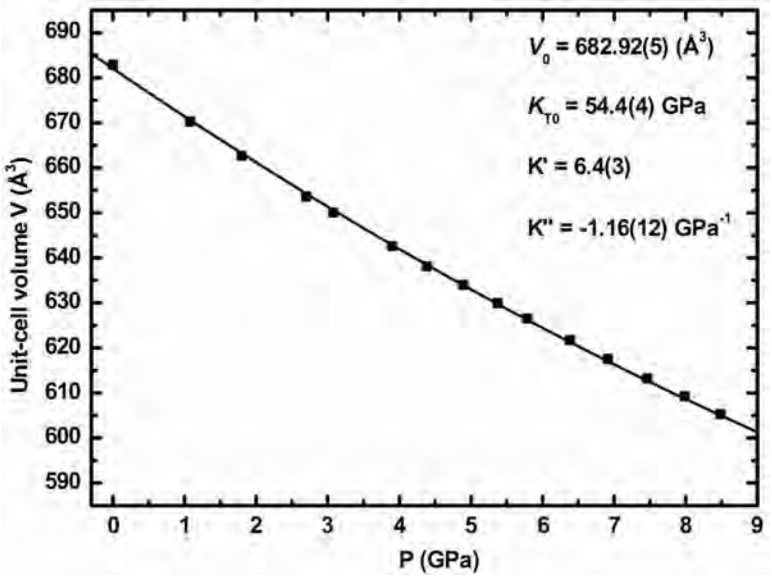

FIG. 2. Evolution of the unit-cell volume as a function of pressure for anorthoclase. The solid curve is the fourth-order Birch–Murnaghan equation of state used to fit the pressure – volume data.

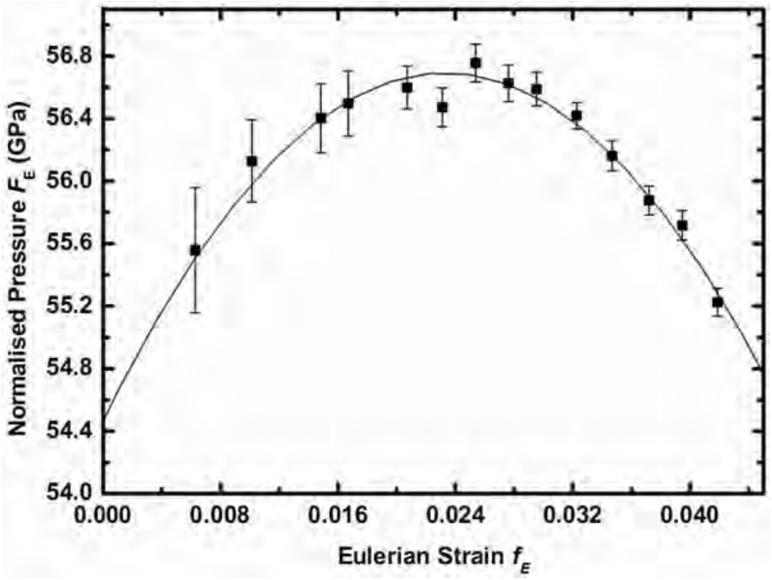

FIG. 3. $F_E - f_E$ plot for anorthoclase ($F_E = P / 3 \times f_E \times (1 + 2f_E)^{5/2}$ and $f_E = [(V_0/V)^{2/3} - 1]$ (Angel 2000). The data fall on a parabolic curve, indicating that only a fourth-order Birch–Murnaghan equation of state can describe the experimental data.

bonded to K]. For the purposes of the current discussion, the *M*–OC(m) and M–OB(m) distances longer than 3 Å are not considered bonded interactions although, as observed by Downs *et al.* (1994), it is difficult to determine whether or not the *M* cation is coordinated to a given O atom in the alkali feldspars.

At high pressures, the configuration of the *M* site of anorthoclase changes significantly. The compression causes a contraction of the volume of the *M* polyhedron by 16% at $P = 6$ GPa. All the *M*–O distances decrease with the exception of *M*–OB(m), *M*–OC(0) and *M*–OD(m), which remain almost constant with pressure. The *M*–OB(0) bond length undergoes the strongest contraction, from 2.80 to 2.48 Å at 6 GPa. This makes the close coordination of the *M* site in anorthoclase much more similar to that of low albite at similar pressures (Benusa *et al.* 2005), with five bonds ranging from 2.24 to 2.53 Å (2.19 to 2.41 Å in albite at 6.5 GPa), but different from microcline in which the *M*–OC(0) distance is shorter at high pressures than *M*–OB(0) (Allan & Angel 1997). Of the longer *M*–O distances, the *M*–OC(m) distance decreases to 2.89 Å at 4.7 GPa and reaches 2.87 Å at 6 GPa, which appears to be an increase in the coordination number of the non-tetrahedrally coordinated cation from 5+1 to 5+2. However, without electron-density calculations (Downs *et al.* 1996, 1999), which are problematic for intermediate compositions, it is very hard to determine whether or not the OC(m) oxygen atom becomes bonded and if the coordination number really increases. Note that the main changes for *M*–OC(m) and *M*–OB(0) distances occur between room pressure and 4.7 GPa; from this pressure to 6 GPa, no significant changes are found, whereas for the other *M*–O distances, the deformation rate remains nearly constant. In this sense, the behavior of anorthoclase reflects that of microcline, in which an unambiguous increase in coordination of the *M* site occurs between 2.9 and 4.4 GPa, with the formation of a K–OB(m) bond (Allan & Angel 1997).

The modifications that occur in the configuration of the *M* polyhedron are represented in Figures 4 and 5. In Figure 4, the shortening of the *M*–OC(m) distance, at $P = 6$ GPa, is shown in a partial projection of the anorthoclase structure along the [001] direction. Figure 5 shows the partial projection of the *M*-site configurations onto the (100) plane at room pressure and at $P = 6$ GPa. The OB(m)–OB(0)–OD(m)–OD(0) quadrilateral lies, as is well known, approximately on (100). The *M*–OB(m) and *M*–OD(m) distances remain almost constant with pressure, while *M*–OB(0) and *M*–OD(0) significantly decrease. The major axis of the displacement ellipsoid of the *M* cation is oriented along the major diagonal of the quadrilateral. The OB(0) – OD(0) distance (minor diagonal) is 5.27 Å at room pressure and 4.88 Å at 6 GPa, whereas the major diagonal does not change. These modifications explain the increase of the α unit-cell angle from 91.8 to 92.5° and the orientation of the displacement ellipsoid of the non-tetrahedrally coordinated cation at 6 GPa.

The framework of tetrahedra. It is well known that in feldspars, the Si,Al tetrahedra behave under pressure as

TABLE 7. LINEAR AXIAL COMPRESSIBILITIES (× 10^{-3} GPa^{-1}), MAGNITUDES (× 10^{-3} GPa^{-1}) AND ORIENTATIONS OF THE PRINCIPAL AXES OF THE STRAIN ELLIPSOIDS FOR ALKALI FELDSPARS IN THE PRESSURE RANGE 0 – 8.5 GPa

	P range GPa	β_a	β_b	β_c		Unit strain	Angle with			ε_1 / $(\varepsilon_1+\varepsilon_2+\varepsilon_3)$
							a	*b*	*c*	
Anorthoclase	0 - 8.5	6.92	2.83	3.91	ε_1	7.4 (1)	22	78	99	53%
this study					ε_2	4.1 (1)	111	68	25	
					ε_3	2.4 (1)	94	26	113	
Low albite	0 - 4.0	7.99	3.00	3.26	ε_1	9.1	25	82	92	60%
Downs *et al.* (1994)					ε_2	3.3	111	110	16	
					ε_3	2.8	103	22	74	
Low albite	0 - 8.4	8.32	2.52	3.16	ε_1	9.2	23	92	94	62%
Benusa *et al.* (2005)					ε_2	3.4	111	121	27	
					ε_3	2.2	98	31	64	
Sanidine	0 - 4.9	8.41	1.63	3.88	ε_1	9.2	23	90	93	63%
Angel *et al.* (1988)					ε_2	3.9	113	90	3	
					ε_3	1.6	90	0	90	
Microcline	0 - 7.1	8.16	0.98	4.07	ε_1	7.7	25	90	90	65%
Allan & Angel (1997)					ε_2	3.4	115	90	1	
					ε_3	0.8	88	0.5	90	

The compressibilities were calculated as $\beta = (d - d_0) / d_0 \times 1/P$, where *d* is a unit-cell parameter. The errors are in the second place after the decimal, and approximately 0.01.

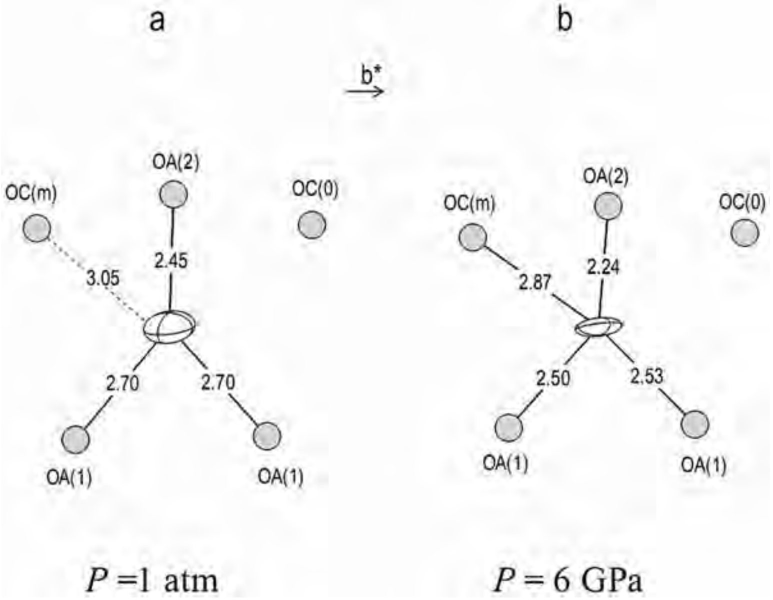

FIG. 4. Partial projections along the [001] direction of the configuration around the non-tetrahedrally coordinated *M* cation in anorthoclase at (a) *P* = 1 atm, and (b) *P* = 6 GPa. The OB and OD oxygen atoms are not shown.

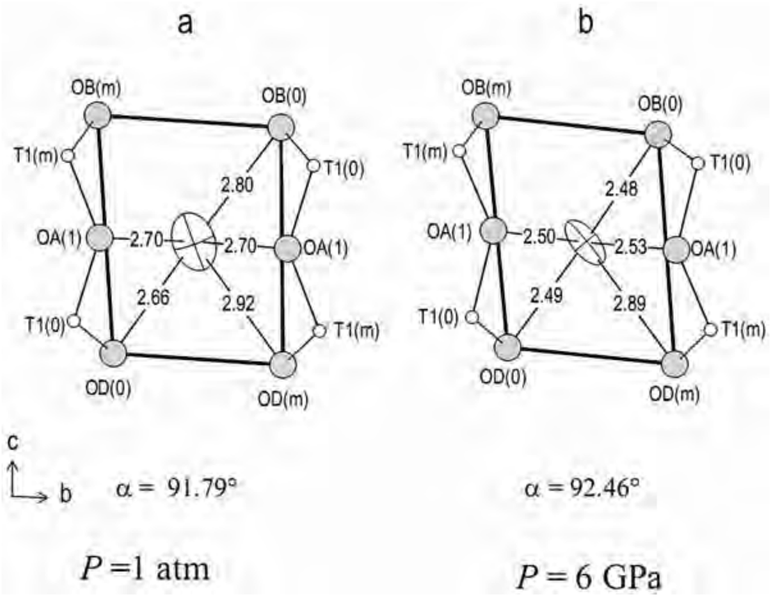

FIG. 5. Partial coordination of the non-tetrahedrally coordinated *M* cation. Projection on the (100) plane at (a) *P* = 1 atm, and (b) *P* = 6 GPa. The OB(m) oxygen atom is not considered to be bonded to the *M* cation.

almost rigid units (*e.g.*, Angel *et al.* 2005). In low albite, there is only a very small reduction in overall < *T*–O > over the entire range of pressure investigated (Downs *et al.* 1994, Benusa *et al.* 2005), whereas in microcline, there is some compression of the *T*1(0) site (Allan & Angel 1997). In the anorthoclase sample studied here, only the *T*1(m) site shows a significant decrease in volume with pressure (Table 4), with compression of the *T*1(m)–O bonds occurring between room pressure and 4.7 GPa, and with no significant further changes from this pressure to 6 GPa.

The O–*T*–O angles in anorthoclase play a minor role in the mechanism of deformation in the crystal structure with pressure (Table 5), with only minor changes of less than 6°. The greatest changes are in the OB(0)–*T*1(0)–OD(0) angle, which increases by 5°, and the OA(1)–*T*1(0)–OB(0) angle, which decreases by about the same amount, both probably as a result of the strong deformation on the *T*2(0)–OB(0)–*T*1(0) angle. The OC(m)–T1(m)–OD(m) angle also increases by 5°, whereas all the other O–*T*–O angles show significantly smaller changes.

Much larger changes are observed in *T*–O–*T* bond angles (Table 6). The *T*1(0)–OB(0)–*T*2(0) angle exhibits the greatest change, with a reduction of 15° between room pressure and 6 GPa, and shows no significant change in the compression rate over the pressure range investigated. In Figure 6a, the four-membered ring of tetrahedra, with (010) as the ring plane, is projected. Whereas the *T*1(0)–OB(0)–*T*2(0) angle decreases (–15°), the *T*1(m)–OD(m)–*T*2(0) angle significantly increases (+7°). These changes could be related to the marked compressional anisotropy on the **ac** plane. In Figure 6b, the other types of fourfold rings of tetrahedra, which lie approximately normal to the **a** axis, are projected onto the $(10\overline{1})$ plane. At *P* = 6 GPa, the *T*1(0)–OC(0)–*T*2(m) angle shows a contraction (–8°), whereas the *T*1(m)–OD(m)–*T*2(0) angle increases (+7°).

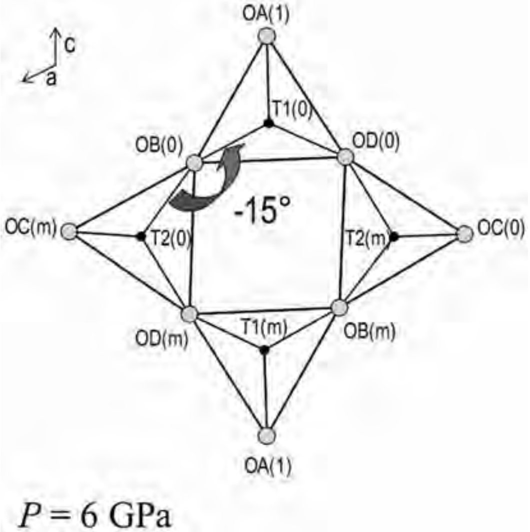

FIG. 6a. The four-membered ring of tetrahedra of the crankshaft chain running parallel to the **a** axis, with (010) as the ring plane. Projection on the **ac** plane (thickness ~3 Å) at *P* = 6 GPa. The ring consists of four symmetrically non-equivalent tetrahedra. Apical oxygen atoms are not shown. The *T*–O–*T* angle, which is most changed by pressure, *T*1(0)–OB(0)–*T*2(0) with a decrease of ~15°, is indicated by the arrow.

Following Allen & Angel (1997), the overall pattern of *T*–O–*T* angle changes in anorthoclase is a “monoclinic” one; the pairs of angles that would be equivalent in a monoclinic structure change in the same way (*e.g.*, both OB angles decrease, both OD angles increase) and can be said to *co-rotate*. A similar behavior was found in microcline (see discussion in Allen & Angel 1997). In contrast, in low albite, the angles at such pairs of oxygen atoms change in opposite directions, or *counter-rotate* in the low-pressure regime, and hence albite displays a distinctly triclinic response to pressure.

CONCLUSIONS

The results indicate that $Ab_{63}Or_{27}An_{10}$ anorthoclase shows a pattern of behavior at high pressure that, in general, is similar to that of the other alkali feldspars, which show about 60% of the overall compression accommodated approximately along the (100) plane normal (Angel 1994). The greatest contribution to the reduction of the cell volume comes from the flexing of the framework of tetrahedra and shortening of the *M*–O distances. There are no phase transitions in anorthoclase up to 8.48 GPa.

When compared to previous studies of end-member alkali feldspars, our results indicate that the response of anorthoclase to pressure is an intriguing mix of the response seen in the end members. Both in terms of the bulk modulus and the elastic anisotropy, anorthoclase is very similar to low albite and much softer and less anisotropic than microcline. The anisotropy appears to be related to the fact that the configuration of the *M* site in anorthoclase at ambient pressure appears to be a slightly expanded version of that of albite, and becomes more like that of albite as pressure increases. However, although the configuration of the *M* site is, of course, determined by the flexing of the framework of tetrahedra, the changes in the framework of anorthoclase with pressure have the distinctly monoclinic pattern found in microcline by Allan & Angel (1997), rather than the triclinic pattern found in albite. In albite, the bending of *T*1(0)–OC(0)–*T*2(m) angle compresses the Na-bearing zigzag channels (Downs *et al.* 1999), whereas anorthoclase and microcline compress by shearing the four-membered rings, which in turn compresses the (K,Na)-bearing channels. In this study, we have therefore confirmed that understanding

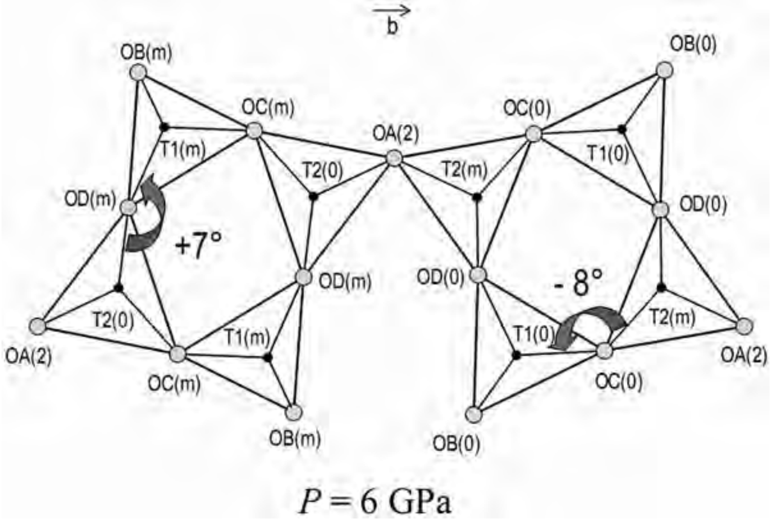

FIG. 6b. The other types of fourfold rings of tetrahedra characteristic of feldspars (those approximately normal to the **a** axis) projected on the $(1\,0\,\bar{1})$ plane at $P = 6$ GPa. Apical oxygen atoms are not shown. Arrows indicate the reduction (–8°) of the $T1(0)$–OC(0)–$T2(m)$ angle and the increase (+7°) of the $T1(m)$–OD(m)–$T2(0)$ angle.

the interplay of compositional change and Al,Si order in determining the elastic and high-pressure response of alkali feldspars requires further detailed study of a number of compositions, including structural determinations of the disordered end-members at high pressures. Once such data are accumulated, they will provide the basis for a more robust development of the thermodynamics of the ternary feldspar solvus at high pressures, and thus the basis for two-feldspar geothermometry.

ACKNOWLEDGEMENTS

The authors thank R.T. Downs, an anonymous referee, and Ian Parsons for their helpful suggestions. Financial support has been provided by MUR – Rome: PRIN 2006047943 to E. Bruno and A. Dal Negro and by NSF grants EAR–0408460 and EAR–0738692 to N.L. Ross and R.J. Angel. We thank P. Gentile, A. Guastoni, R. Carampin and L. Tauro for helping in the preparation and chemical analysis of the sample. The authors thank the Interdepartmental Center "G. Scansetti" for a grant from Compagnia di San Paolo, Torino. This paper is dedicated to the memory of J.V. Smith for his unequalled contributions to the understanding of the complexities of feldspars.

REFERENCES

ALLAN, D.R. & ANGEL, R.J. (1997): A high-pressure structural study of microcline ($KAlSi_3O_8$) to 7 GPa. *Eur. J. Mineral.* **9**, 263-275.

ANGEL, R.J. (1994): Feldspars at high pressure. *In* Feldspars and their Reactions (I. Parsons, ed.). Kluwer, Dordrecht, The Netherlands (271-312).

ANGEL, R.J. (2000): Equations of state. *In* High-Temperature and High-Pressure Crystal Chemistry (R.M. Hazen & R.T. Downs, eds.). *Rev. Mineral. Geochem.* **41**, 35-59.

ANGEL, R.J., ALLAN, D.R., MILETICH, R. & FINGER, L.W. (1997): The use of quartz as an internal pressure standard in high-pressure crystallography. *J. Appl. Crystallogr.* **30**, 461-466.

ANGEL, R.J., DOWNS, R.T. & FINGER, L.W. (2000): High-temperature – high-pressure diffractometry. *In* High-Temperature and High-Pressure Crystal Chemistry (R.M. Hazen & R.T. Downs, eds.). *Rev. Mineral. Geochem.* **41**, 559-596.

ANGEL, R.J., HAZEN, R.M., MCCORMICK, T.C., PREWITT, C.T. & SMYTH, J.R. (1988): Comparative compressibility of end-member feldspars. *Phys. Chem. Minerals* **15**, 313-318.

ANGEL, R.J., ROSS, N.L. & ZHAO, JING (2005): The compression of framework minerals: beyond rigid polyhedra. *Eur. J. Mineral.* **17**, 193-199.

BENNA, P., NESTOLA, F., BOFFA BALLARAN, T., BALIĆ-ŽUNIĆ, T., LUNDEGAARD, L.F. & BRUNO, E. (2007): The high-pressure structural configurations of $Ca_{0.2}Sr_{0.8}Al_2Si_2O_8$ feldspar: the $I\bar{1} - I2/c$ and $I2/c - P2_1/c$ phase transitions. *Am. Mineral.* **92**, 1190-1199.

Benusa, M.D., Angel, R.J. & Ross, N.L. (2005): Compression of albite, $NaAlSi_3O_8$. *Am. Mineral.* **90**, 1115-1120.

Downs, R.T., Andalman, A. & Hudacsko, M. (1996): The coordination numbers of Na and K atoms in low albite and microcline as determined from a procrystal electron-density distribution. *Am. Mineral.* **81**, 1344-1349.

Downs, R.T., Hazen, R.M. & Finger, L.W. (1994): The high-pressure crystal chemistry of low albite and the origin of the pressure dependency of Al–Si ordering. *Am. Mineral.* **79**, 1042-1052.

Downs, R.T., Yang, H., Hazen, R.M., Finger, L.W. & Prewitt, C.T. (1999): Compressibility mechanisms of alkali feldspars: new data from reedmergnerite. *Am. Mineral.* **84**, 333-340.

Harlow, G.E. (1982): The anorthoclase structures: the effects of temperature and composition. *Am. Mineral.* **67**, 975-996.

Hazen, R.M. (1976): Sanidine: predicted and observed monoclinic-to-triclinic reversible transformations at high pressure. *Science* **194**, 105-107.

King, H.E., Jr. & Finger, L.W. (1979): Diffracted beam crystal centering and its application to high pressure crystallography. *J. Appl. Crystallogr.* **12**, 374-378.

Miletich, R., Allan, D.R. & Kuhs, W.F. (2000): High-pressure single-crystal technique. *In* High-Temperature and High-Pressure Crystal Chemistry (R.M. Hazen & R.T. Downs, eds.). *Rev. Mineral. Geochem.* **41**, 445-520.

Nestola, F., Boffa Ballaran, T., Benna, P., Tribaudino, M. & Bruno, E. (2004): High-pressure phase transitions in $Ca_{0.2}Sr_{0.8}Al_2Si_2O_8$ feldspar. *Am. Mineral.* **89**, 1474-1479.

Ohashi, Y. (1982): A program to calculate the strain tensor from two sets of unit-cell parameters. *In* Comparative Crystal Chemistry (R.M. Hazen & L.W. Finger, eds.). John Wiley & Sons, Chichester, U.K. (92-102).

Sheldrick, G.M. (2008): A short history of SHELX. *Acta Crystallogr.* **A64**, 112-122.

Smith, J.V. (1974a): *Feldspar Minerals.* 1. *Crystal Structure and Physical Properties.* Springer-Verlag, Berlin, Germany.

Smith, J.V. (1974b): *Feldspar Minerals.* 2. Chemical and Textural Properties. Springer-Verlag, Berlin, Germany.

Smith, J.V. & Brown, W.L. (1988): *Feldspar Minerals.* 1. *Crystal Structures, Physical, Chemical and Microtextural Properties* (second revised and extended ed.). Springer-Verlag, Berlin, Germany.

Smith, J.V. & MacKenzie, W.S. (1954): Further complexities in the lamellar structure of alkali feldspars. *Acta Crystallogr.* **7**, 380-381.

Stoe & Cie (1999): *Crystal Optimization for Numerical Absorption Correction.* Stoe and Cie GmbH, Darmstad, Germany.

Stoe & Cie (2001): *Data Reduction Program.* Stoe and Cie GmbH, Darmstad, Germany.

Tenner, T.J., Lange, R.A & Downs, R.T. (2007): The albite fusion curve re-examined: new experiments and the high-pressure density and compressibility of high albite and $NaAlSi_3O_8$ liquid. *Am. Mineral.* **92**, 1573-1585.

Received November 22, 2007, revised manuscript accepted November 27, 2008.